Front. Med. 2019, 13(3): 398–408
https://doi.org/10.1007/s11684-019-0689-5

RESEARCH ARTICLE

Urotensin II receptor antagonist reduces hepatic resistance and portal pressure through enhanced eNOS-dependent HSC vasodilatation in CCl_4-induced cirrhotic rats

Ruoxi Zhang[1], Jing Chen[2], Diangang Liu (✉)[1], Yu Wang[3]

[1]*Department of General Surgery, Xuanwu Hospital, Capital Medical University, Beijing 100053, China;* [2]*Department of Gastroenterology, the Second Affiliated Hospital of Harbin Medical University, Harbin 150010, China;* [3]*Department of General Surgery, Beijing Friendship Hospital, Capital Medical University, Beijing 100050, China*

Abstract **Increased serum urotensin II (UII) levels in human cirrhotic populations have been recently shown, but the long-term effects of UII receptor antagonist on the cirrhosis have not been investigated. To investigate the therapeutic effects of urotensin II receptor (UT) antagonist palosuran on rats with carbon tetrachloride (CCl_4)-induced cirrhosis, the hepatic and systemic hemodynamics, liver fibrosis, the metalloproteinase-13 (MMP-13)/tissue inhibitor of metalloproteinase-1 (TIMP-1) ratio, hepatic Rho-kinase activity, and the endothelial nitric oxide synthase (eNOS) activity are measured in CCl_4-cirrhotic rats treated with palosuran or vehicle for 4 weeks. Primary hepatic stellate cells (HSCs) are used to investigate the changes in UII/UT expression and the *in vitro* effect of palosuran. Compared with the vehicle-treated cirrhotic rats, treatment with palosuran can reduce the portal pressure (PP), decrease the risk of liver fibrosis and the level of α smooth muscle actin, collagen-I (COL-I), and transforming growth factor β expression. However, treatment with palosuran can increase MMP-13/TIMP-1, p-vasodilator-stimulated phosphoprotein (p-VASP), and p-eNOS expression. Moreover, *in vitro* UII/UT mRNA expression increases during HSC activation. MMP-13/TIMP-1, COL-I, and p-VASP are inhibited after palosuran treatment. Our data indicate that long-term administration of palosuran can decrease PP in cirrhosis, which results from decreased hepatic fibrosis and enhanced eNOS-dependent HSC vasodilatation.**

Keywords portal hypertension; cirrhosis; urotensin II; palosuran; hepatic stellate cell

Introduction

Portal hypertension (PH) is a contributing factor of morbidity and mortality in patients with liver cirrhosis. The initial event, referred to as intrahepatic resistance (IHR), causes increased portal pressure (PP) and develops PH in patients with cirrhosis. Increased IHR is the main result of hepatic architectural distortion caused by regenerative nodules, fibrosis, and increased hepatic vascular tone (a functional, nonstructural component of IHR located within sinusoidal blood circulation) [1].

Hepatic stellate cells (HSCs) play an important role in the pathophysiology of increased IHR through their contractile properties and elevated collagen production [2–4]. Previous studies illustrated that numerous vasoconstrictors participate in the increased vascular tone process in patients with hepatic fibrosis [5–7]; angiotensin II (Ang II) is an example. A somatostatin-like cyclic undecapeptide called urotensin II (UII) is a highly potent vasoconstrictor, which is more effective in constricting blood vessels than any other substance [8]. Along with the study of UII and the novel G-protein-coupled receptor GPR14 (known as UT) system in human diseases, UII is the ligand for the UT [8–10]. Moreover, UII possesses mitogenic and fibrogenic potential [11]. The UII/UT system expression increases in patients with PH. In these patients, UII serum levels have a positive correlation with free PP [12]. Meanwhile, another UT inhibitor, SB-71041, stops the process of fibrosis in cirrhotic rats induced by CCl_4, and UII induces HSC proliferation [13]. Thus, manipulating the UII/UT system pathways may be a successful strategy for treating PH in cirrhosis patients.

Palosuran (4-ureido-quinoline derivate, ACT-058362) is a specific, nonpeptide, competitive UT receptor antagonist

Received April 8, 2018; accepted December 27, 2018
Correspondence: Diangang Liu, liudiangang01@gmail.com

[14]. However, its capability to stop or even reverse fibrosis progression and its long-term hemodynamic effect in cirrhotic rats has not yet been measured. In this study, the long-term efficacy of palosuran administration on hemodynamics in CCl_4-cirrhotic rats is studied and tested.

Materials and methods

Animals

Male Wistar rats (weighing 60–75 g) were used in a cirrhosis model induced by carbon tetrachloride inhalation (CCl_4, Beijing Chemical Factory, Beijing, China) thrice per week. Phenobarbital (0.3 g/L) was another component used in the drinking water to assist the experimental process, following a previously described method [15]. When cirrhotic rats developed ascites after 12 weeks, CCl_4 and phenobarbital administration were stopped, and treatment was started 1 week later. Animals were taken from the Animal Center (Beijing, China). The Animal Care and Use Committee of Capital Medical University approved all protocols and procedures (Permit Number: 50-2010). Animals were raised in a controlled environment (typically in the range of 23 °C to 25 °C) with 12 h of light and dark exposure 1 day before the experiment. Animals received unlimited food and water intake during the study.

Experimental groups

The rats were separated into three groups, namely, normal group, control group, and treatment group. The normal group remained untreated ($n = 6$). Male rats with cirrhosis were allocated to the control group or treatment group randomly, and they received placebo or UT antagonist (palosuran), respectively, for 4 weeks (300 mg/kg body weight per day) (ACT-058362; kindly provided by Actelion Pharmaceuticals Ltd., Allschwil, Switzerland). The dosage of palosuran was administered based on previous studies [16].

After the hemodynamic studies, each rat liver was extracted. Blood was extracted via cardiac puncture and centrifuged. The serum was preserved at temperature of − 80 °C. The liver samples were snap-frozen and stored in liquid nitrogen until analysis for hydroxyproline (Hyp) and total RNA extraction. The remaining hepatic tissues were prepared for histological examination by being placed in a 10% formalin solution and embedded into paraffin blocks.

Hemodynamic studies

Twenty-four hours after the last dose of palosuran or vehicle, water was removed for 12 h. Hemodynamic studies were performed under ketamine (100 mg/kg) and midazolam (5 mg/kg) anesthesia; moreover, body temperature was maintained at 37 °C ± 0.5 °C. Hemodynamic evaluation of PH was performed as previously mentioned [17,18]. PE-50 catheters were inserted into the femoral artery and ileocolic vein to measure the mean arterial pressure (mmHg) and PP (mmHg) in a constant manner. The portal vein blood flow (PBF) was measured by using a T206 blood flowmeter (Transonic Systems; Ithaca, NY, USA) situated as close as possible to the liver through the portal vein. An ARIA pressure conductance system (Millar Instruments, Houston, TX, USA) with a Powerlab/4SP analog-to-digital converter (AD Instruments, Oxfordshire, UK) was utilized to measure the blood pressure and flow. Intrahepatic vascular resistance was calculated as PP/PBF.

Evaluation of hepatic fibrosis

Histological analysis

Hematoxylin and eosin (H&E), Gordon and Sweet's reticulin, and Masson's trichrome (G&S and M) staining methods were used to stain the liver specimens (5 μm) that were drop-fixed in the formalin solution. Fibrosis was then histologically analyzed according to a fibrosis scoring system [13,19]. Immunohistochemical staining and semi-quantitative analysis of immunopositive cells that tested positive for α-smooth muscle actin (α-SMA) and transforming growth factor-β1 (TGF-β1) were performed as mentioned [12].

Measurement of liver Hyp content

Liver Hyp was tested by means of a Hyp detection kit (Jiancheng Institute of Biotechnology, Nanjing, China) in accordance with the manufacturer's instructions. The Hyp content was recorded in mg/g of wet liver.

Evaluation of hepatic function

Hepatic function was assessed by the following substances: serum alanine aminotransferase, aspartate aminotransferase (AST), total bilirubin (TBIL), and albumin (ALB) were measured by using an automatic biochemical analyzer (7600; HITEC, Japan).

Assessment of nitric oxide bioavailability

Nitric oxide (NO) bioavailability was assessed through its surrogate marker called phosphorylated vasodilator-stimulated phosphoprotein (p-VASP, Ser-239), which is a sensitive indicator of protein kinase G (PKG) activity [20]. The phosphorylated form of eNOS (Ser1176) indirectly reflected hepatic NO synthase activity, and p-VASP and eNOS levels were quantified by Western blot analysis.

Quantitative real-time PCR (qPCR)

As previously described, RNA extraction and cDNA synthesis were performed in this study [14]. UII, UT, collagen I, metalloproteinase-13 (MMP-13), and tissue inhibitor of metalloproteinase-1 (TIMP-1) gene expression were quantified by real-time PCR. A housekeeping gene, glyceraldehyde-3-phosphate dehydrogenase, was used as an internal control for target genes. The primer sequences are shown in Table 1, and all primers were obtained from Invitrogen (Beijing, China). SYBR Green real-time PCR (Applied Biosystems) was selected to examine mRNA expression using an ABI 7500 instrument (Applied Biosystems). PCR was performed in a 20 μL reaction mixture containing 2 μg cDNA, 1 μL of each primer, and 10 μL SYBR Green PCR Master Mix. qPCR analysis was performed, and the recorded, normalized values were the average of three replicates [21].

Western blot analysis

Western blot analysis and protein extraction were performed as previously mentioned [12,13]. The sample was ground into cell powder and transferred to a 5 mL centrifuge tube. Four volumes of lysis buffer (8 mol/L urea, 1% Protease Inhibitor Cocktail) was added to the cell powder, followed by sonication three times on ice using a high-intensity ultrasonic processor (Scientz). The remaining debris was removed by centrifugation at 12 000 × *g* at 4 °C for 10 min. The bicinchoninic acid assay (Pierce BCA Protein Assay kit; Thermo Fisher Scientific Inc., Rockford, IL, USA) was adopted to test proteins that were harvested from liver specimens (Protein Extractor IV; DBI, Shanghai, China). Protein specimens (about 20 μg) were disposed by SDS-PAGE, which was a method that contained two steps. First, samples were taken at 80 V for a duration of 40 min on a 5% acrylamide stacking gel and at 120 V for a duration of 70 min on a 10% running gel. The specimens were then placed (390 mA for 70 min) on a nitrocellulose membrane purchased from Amersham Biosciences (Hybond-C Extra Membrane 45, Uppsala, Sweden). The nitrocellulose membranes were infiltrated in Tris-buffered saline composed with 10 mmol/L Tris-HCl and 250 mmol/L NaCl supplemented with 5% powdered non-fat milk and 0.1% Tween-20 for 2 h to block nonspecific sites and incubated with a primary antibody called p-eNOS (Ser 1176, Cell Signaling, Danvers, MA, USA) and p-VASP (Ser-239, Calbiochem, San Diego, CA, USA) overnight at a temperature of 4 °C in blocking solution. The final blots were placed in room temperature for 2 h after the blots were washed and incubated with a secondary antibody (HRP-linked goat anti-rabbit IgG). An enhanced chemiluminescence kit (Thermo Fisher Scientific, Shanghai, China) was applied to make immunoreactivity visible, the film was scanned using a Bio-Rad imaging system, and the bands were analyzed using Quantity One software (Bio-Rad, USA). Protein expression was normalized to β-actin expression.

Enzyme linked immunosorbent assay (ELISA) analysis

Concentrations of UII, COL-I, MMP-13, and TIMP-1 in rat serum and HSC supernatant were quantified with ELISA (Bio-Rad Laboratories, Richmond, CA, USA) [13] (Phoenix Biotech Co., Ltd, Beijing, China for UII; Sigma–Aldrich Co. LLC for COL-I, MMP-13, and TIMP-1).

Table 1 Primers for quantitative real-time PCR analysis

Gene	Primer sequence	Size (bp)	Accession number
GADPH	F: 5′-CCTGCCAAGTATGATGACATCAAGA-3′ R: 5′- GTAGCCCAGGATGCCCTTTAGT-3′	75	BC059110.1
UII	F: 5′-CAGAAGCAGAGGGAAGCCTA-3′ R: 5′-CAAGCTTCCCCTTGGAGTG-3′	68	NM_019160
UT	F: 5′-CATTGGGCTGCTCTATGTCC-3′ R: 5′-AAAGAAGCTTGCTGAGATAGCC-3′	60	NM_020537
COL-I	F: 5′- CCTTTCTCCACCCCCTCTT-3′ R: 5′- TGTGTCTTTGGGGGAGACTT-3′	69	NM_053304.1
MMP-13	F: 5′- CCCTGGAGCCCTGATGTTT-3′ R: 5′- CTCTGGTGTTTTGGGGTGCT-3′	75	NM_133530.1
TIMP-1	F: 5′- CAGCAAAAGGCCTTCGTAAA-3′ R: 5′- TGGCTGAACAGGGAAACACT-3′	70	NM_053819.1
α-SMA	F: 5′- TGCCATGTATGTGGCTATTCA-3′ R: 5′- ACCAGTTGTACGTCCAGAAGC-3′	61	NM_001613.2
TGF-β1	F: 5′- CCTGGAAAGGGCTCAACAC-3′ R: 5′- CTGCCGTACACAGCAGTTCT-3′	100	NM_021578.2

Abbreviations: GAPDH, glyceraldehyde phosphate dehydrogenase; UII, urotensin II; UT, urotensin II receptor; COL-I, collagen type I; MMP-13, metalloproteinase-13; TIMP-1, tissue inhibitor of metalloproteinases-1; α-SMA, α-smooth muscle actin; TGF-β1, transforming growth factor 1; F, forward; R, reverse.

Effect of palosuran on isolated, primary HSCs

Normal male rats (Wistar rats, 450–550 g body weight) experienced stellate cell isolation using pronase and collagenase (Boehringer Mannheim, Indianapolis, IN, USA), as previously mentioned [22–24]. Hepatocytes were briefly isolated through a procedure called isolated hepatic profusion with 0.05% IV collagenase (Sigma), followed by elutriatrion. Non-parenchymal cells were isolated by *in situ* liver perfusion with 0.05% collagenase and 0.1% E pronase (Roche), followed by separation on a discontinuous Nycodenz (Sigma) density gradient, and stellate cells were removed from the top layer of the gradient. Primary HSCs were treated with different palosuran doses (0 mol/L, 0.25×10^{-5} mol/L, 0.5×10^{-5} mol/L, and 1×10^{-5} mol/L). After 24 h, the cells were lysed, and the total RNA and protein were extracted using the TRIzol reagents and protein lysis, respectively. UII, MMP13, TIMP-1, and COL-I mRNA levels were measured through qPCR and analyzed semiquantitatively. The MMP13, TIMP-1, and COL-I protein levels in the HSC supernatant were measured using an ELISA analysis. p-VASP and p-eNOS protein expression in HSCs was detected through a Western blot analysis.

Statistical analysis

The results are presented as mean ± SD. Comparisons were made by the unpaired Student's *t*-test and one-way analysis of variance followed by the Student Newman–Keuls test technique. The statistical program IBM SPSS Statistics 20.0 (IBM Corporation, Somer, NY, USA) was used to analyze the data. A P-value < 0.05 was considered statistically significant.

Results

Long-term effects of late palosuran administration

Hemodynamic effects

As expected, PP and superior mesenteric artery (SMA) flow greatly increased in CCl_4 rats compared with normal rats (Table 2). Palosuran administration caused a 34% reduction in PP, which was significant ($P = 0.002$). In the splanchnic area, palosuran decreased SMA flow and HVR resistance ($P = 0.026$ and $P = 0.013$, respectively).

A comparison of cirrhotic rats and normal rats shows that MAP was significantly lower ($P = 0.003$), and no significant changes of MAP and HR were observed in palosuran-treated cirrhotic rats compared with the vehicle group.

Biochemistry parameters

An increase in biochemical parameters was observed in CCl_4 rats compared with normal rats; those parameters

Table 2 Effects of palosuran on hepatic and systemic hemodynamics in CCl_4-cirrhotic rats

	Normal $n = 6$	Vehicle $n = 10$	Palosuran $n = 10$
HR (beats/min)	438.25±14.66	447.25±11.13	442.00±14.45
MAP (mmHg)	113.38±12.86	78.25±11.30$^{\#}$	89.25±10.78
PP (mmHg)	8.00±1.31	17.13±2.42	11.25±1.03*
Portal flow ($mL \cdot min^{-1} \cdot 100\ g^{-1}$)	6.51±0.32	6.85±0.39	7.20±0.44
SMA flow ($mL \cdot min^{-1} \cdot 100\ g^{-1}$)	1.9±0.12	5.1±0.21	3.2±0.23*
HVR ($mmHg \cdot mL^{-1} \cdot min \cdot 100\ g$)	1.3±0.14	2.5±0.23	1.4±0.10*
Body weight (g)	450±11.23	387±10.11	392±12.34

*$P<0.05$, palosuran-treated group versus vehicle group; $^{\#}P<0.05$, vehicle group versus normal; HR, heart rate; MAP, mean arterial pressure; PP, portal pressure; SMA, superior mesenteric artery; HVR, hepatic vascular resistance; Values are expressed as mean±SD.

Table 3 Effects of palosuran on biochemical parameters in CCl_4-cirrhotic rats

	Normal $n = 6$	Vehicle $n = 10$	Palosuran $n = 10$
AST (IU/L)	98.63±28.75	2242.86±560.67$^{\#}$	1288.42±350.29*
ALT (IU/L)	36.76±6.36	932.05±213.89$^{\#}$	538.10±53.55*
TBIL (mg/dL)	0.61±0.17	25.54±5.33$^{\#}$	18.618±2.85
ALB (g/L)	31.06±3.03	27.63±2.39	28.38±2.67

AST, aspartate aminotransferase; ALT, serum alanine aminotransferase; TBIL, total bilirubin; ALB, albumin. *$P<0.05$, palosuran-treated group versus vehicle group; $^{\#}P<0.05$, vehicle group versus normal.

include alanine aminotransferase (ALT), AST, and TBIL (Table 3). A comparison with the vehicle group shows that palosuran significantly decreased AST and ALT levels ($P = 0.023$ and $P = 0.034$, respectively) and had a slight influence on TBIL ($P = 0.31$).

Liver fibrosis

The histopathologic results of hepatic rat tissues are displayed in Fig. 1. The histological detection of cirrhotic rats fed by CCl_4 demonstrated massive steatosis, gross necrosis, and broad inflammation cell infiltration (Fig. 1A, H&E). The severity of hepatic fibrosis was more distinct, characterized by histopathologic alterations including thick and often formed fibrotic centro-central septa (Fig. 1A, G&S and M). Using UII receptor antagonist, palosuran, can lead to a lower mean fibrosis score (Table 4) compared with the cirrhosis group (Fig. 1B). Hyp quantification was chosen to test hepatic collagen, and the liver Hyp concentration in the cirrhosis group was higher than that within the normal group. A comparison of the cirrhosis group and the palosuran group ($P < 0.01$) was made, and findings reflect that the level of liver Hyp in the cirrhosis group was higher than that of the palosuran group ($P < 0.01$; Fig. 1C). The same result was observed in liver COL-I mRNA levels and serum concentrations (Fig. 1D). The α-SMA-positive cells and the TGF-β1-positive cells were tested to confirm that palosuran treatment eliminated liver fibrosis and improved liver cirrhosis induced by CCl_4. Morphometric analysis (Fig. 1A, α-SMA, TGF-β1) confirmed that the administration of palosuran markedly improved the region filled with α-SMA-positive cells (Fig. 1E) and TGF-β1 cells (Fig. 1F) compared with the vehicle-treated cirrhotic rats.

Serum UII and serum matrix metalloproteinase-13 and tissue inhibitor of metalloproteinase-1 levels

The rats experiencing cirrhosis had increased UII and MMP-13 concentrations in serum compared with normal rats and those within the control group. Rats that were administered palosuran had a large decrease in serum UII and serum MMP-13 levels (Fig. 2A and 2C; $P < 0.05$). No significant difference in serum TIMP-1 levels was observed among the three groups (Fig. 2C), but the palosuran-treated subjects tended to show significantly increased MMP-13 and TIMP-1 ratio (Fig. 2E).

Changes in hepatic UII, UT, TIMP-1, and MMP-13 mRNA expression

qPCR determined that UII/UT mRNA gene expression significantly increased hepatic tissue in CCl_4 cirrhotic rats compared with the normal group (Fig. 2B; $P < 0.05$). In the palosuran-treated group, UII/UT mRNA levels in hepatic tissue were expressed at a slower rate than in the cirrhotic rats (Fig. 2B; $P < 0.05$). We examined hepatic TIMP-1 and MMP-13 mRNA levels to determine the extent in which palosuran may slow down or even stop the progression of CCl_4-fibrosis. The concentrations of TIMP-1 and MMP-13 mRNA were significantly higher in cirrhotic rats than in the control group. Palosuran administration increased the MMP-13/TIMP-1 ratio (Fig. 2D and 2E).

Palosuran improves eNOS activity

To clarify which mechanism was partially responsible for the decreasing PP, the p-VASP and p-eNOS expression in CCl_4 cirrhotic rat livers were characterized, and results suggested that eNOS enzymatic activity was involved in cirrhotic PH. Western blot analysis revealed lower p-eNOS in CCl_4 cirrhotic rats compared with normal controls, but no change was observed in p-VASP levels (Fig. 2F and 2G). Overall, palosuran-treated cells significantly increased p-VASP and p-eNOS levels compared with vehicle-treated cirrhotic rats (Fig. 2F and 2G).

Direct effect of palosuran on primary HSCs of normal rats in vitro

Trypan blue staining indicated that cell viability was 90%. Primary HSCs were small, round, and had a quiescent phenotype at 48 h. Additionally, the HSCs had blue-green intrinsic autofluorescence when they were stimulated at a 327 nm wavelength. The purity of isolated HSCs was determined by means of morphology and fluorescence staining using α-SMA (Fig. 3A). To evaluate the effect of palosuran on HSCs *in vitro*, the cells were first cultured with 0 mol/L, 0.25×10^{-5} mol/L, 0.5×10^{-5} mol/L, and 1×10^{-5} mol/L of palosuran for 24 h. UII gene expression was upregulated during HSC activation (α-SMA as indicated by measurement of its activation). After an incubation period of 7 days, UII expression increased to 400% compared with freshly isolated cells (Fig. 3B; $P < 0.05$). Palosuran concentrations of 1×10^{-5} mol/L, 0.5×10^{-5} mol/L, and 0.25×10^{-5} mol/L significantly downregulated COL-I gene expression in HSCs and protein expression in HSC cell supernatant (Fig. 3C).

Palosuran significantly increased the MMP-13 gene expression in HSCs and in its supernatant, which was overall dose-dependent (Fig. 3D). Palosuran significantly decreased the TIMP-1 gene expression measured by ELISA only in the presence of palosuran at 1×10^{-5} mol/L ($P < 0.05$; Fig. 3E). Furthermore, the Western blot analysis revealed an increase in the p-VASP gene expression in palosuran-treated HSCs (Fig. 3F).

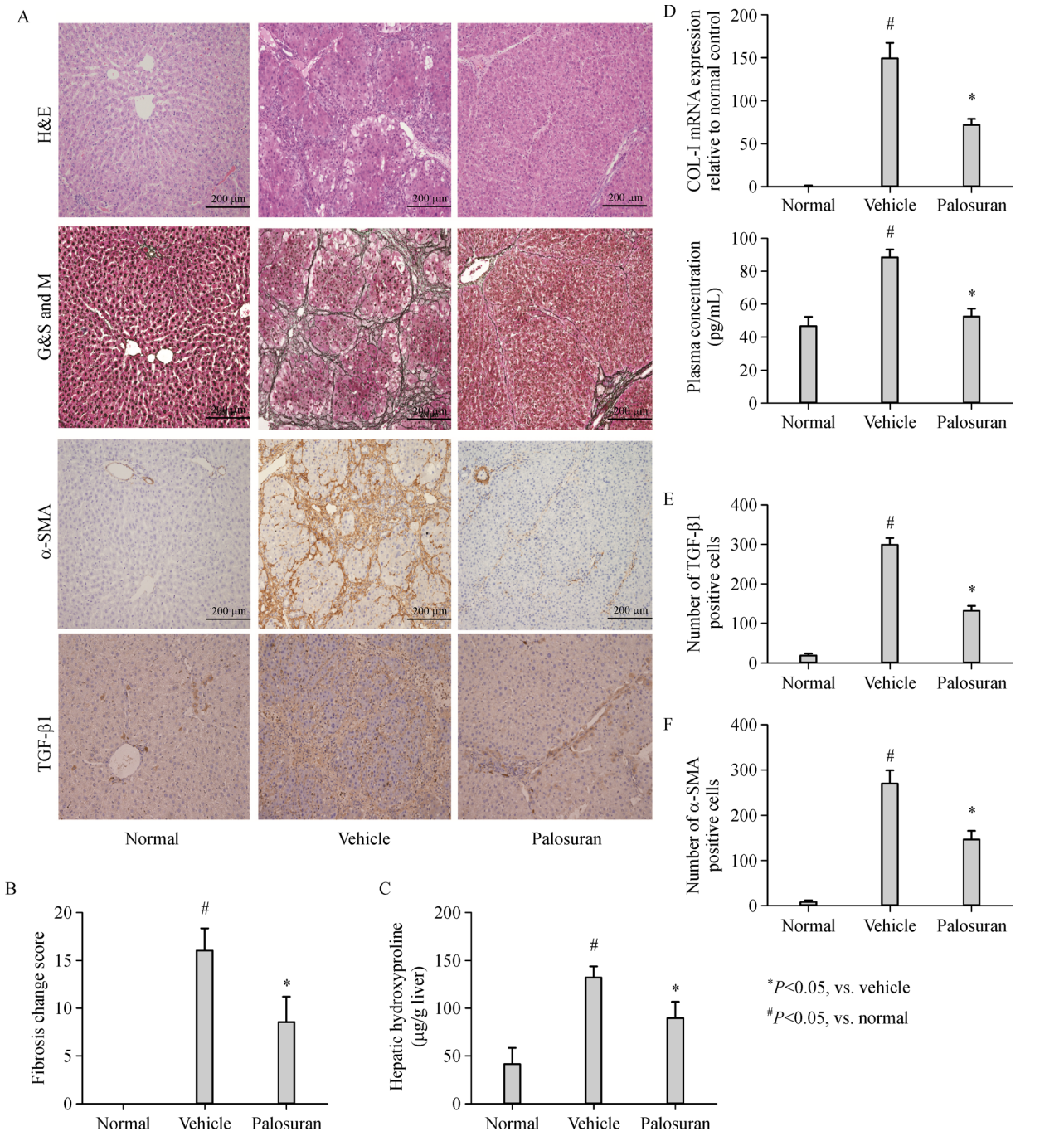

Fig. 1 Reduction of hepatic fibrosis with palosuran treatment. (A) Histologic findings ((H&E, Gordon–Sweet reticulum and Masson trichrome, immunohistochemistry): a comparison of liver architecture of normal control, extensive portal-portal and portal-central fibrous linkage, distortion of liver architecture and marked regeneration nodules showed much more positive expressions for α-SMA and TGF-β1 were observed. (B) Palosuran treatment markedly reduced liver fibrosis change score compared with vehicle group. (C) Hepatic Hyp concentrations in the three experimental groups were analyzed by the sample alkaline hydrolysis method. (D) COL-I mRNA in rat liver tissue and plasma COL-I concentration. (E) Number of α-SMA positive cells. (F) Number of TGF-β1 positive cells. *$P < 0.05$, compared with the vehicle; #$P < 0.05$, compared with the normal control group.

Table 4 Fibrosis change score of CCl_4-induced cirrhosis treated with palosuran

Group	Fibrosis score						
	0	1	2	3	4	5	6
Normal	6	0	0	0	0	0	0
Vehicle[a]	0	0	0	0	2	4	4
Treatment[b]	0	0	4	3	3	0	0

Stages 0, I, II, III, IV, V, and VI represent scores of 0–6, respectively. The mean of scores were calculated by multiplying the number of animals by their individual score and dividing sum scores by the number of rats in each group ([a]$P<0.01$, compared with the normal group; [b]$P<0.01$, compared with the normal and vehicle group).

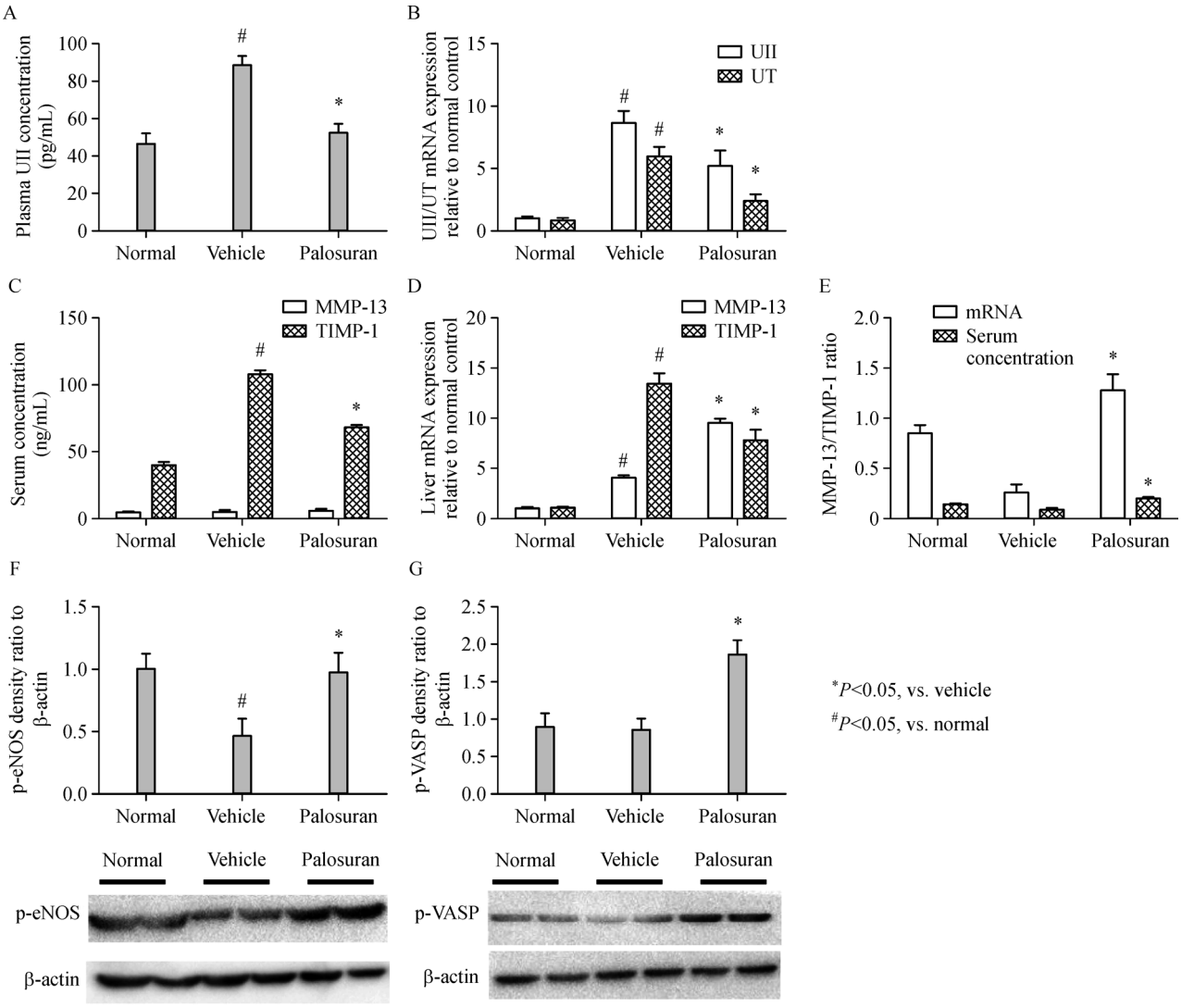

Fig. 2 Effects of palosuran on UII/UT system, MMP-13/TIMP-1, Rho-kinase, and eNOS pathways in CCl_4-cirrhotic rats. (A) Plasma UII was upregulated in CCl_4-cirrhotic rats, and UII levels were significantly decreased in palosuran-treated groups compared with vehicle group. $^*P < 0.05$, versus vehicle. (B) UII/UT mRNAs in liver were upregulated in CCl_4-cirrhotic rats, and UII/UT mRNAs were markedly reduced in palosuran-treated group. (C) Serum MMP-13 and TIMP-1 concentration levels in CCl_4-cirrhotic rats treated with vehicle or palosuran. MMP-13 was upregulated in CCl_4-cirrhotic rats, and MMP-13 levels were significantly decreased in palosuran-treated groups compared with vehicle group. TIMP-1 levels were not significantly different among groups. (D) MMP-13 and TIMP-I mRNAs in liver were upregulated in CCl_4-cirrhotic rats, and palosuran treatment tended to decrease expression of MMP-13 and TIMP-1 mRNAs. (E) Palosuran treatment tended to attenuate the increase in ratio of MMP-13/TIMP-1 compared with the vehicle group. (F) Western blot analysis revealed a decreased p-eNOS in CCl_4 cirrhotic rats compared with the normal controls, and palosuran treatment significantly increased p-eNOS. (G) p-VASP levels were not significantly different between normal group and vehicle group. Palosuran treatment significantly increased p-VASP compared with vehicle-treated cirrhotic rats. $^*P < 0.05$, versus vehicle; $^{\#}P < 0.05$, versus normal.

Discussion

This study and recent other studies demonstrate that UII serum concentration is increased in patients with hepatic sclerosis and PH [12,25]. UII serum levels show a positive correlation with PP [12]. In animal studies, exogenous UII potentially induced hepatic fibrosis and elevated PP in hepatic fibrosis compared with normal rats [26]. However, the mechanism and long-term effects of the late UII receptor antagonist administration in the treatment of cirrhosis are obscured. In this study, we select palosuran, a non-peptide, oral, and selective UT receptor antagonist, which is the first in its class to be tested in humans [27].

This study shows that palosuran reduced PP in CCl_4 cirrhotic rats. The decreased PP is not linked to modifications in PBF, which would suggest a reduction in vascular resistance within the liver. Palosuran administration has a beneficial effect on hepatic resistance, which could be

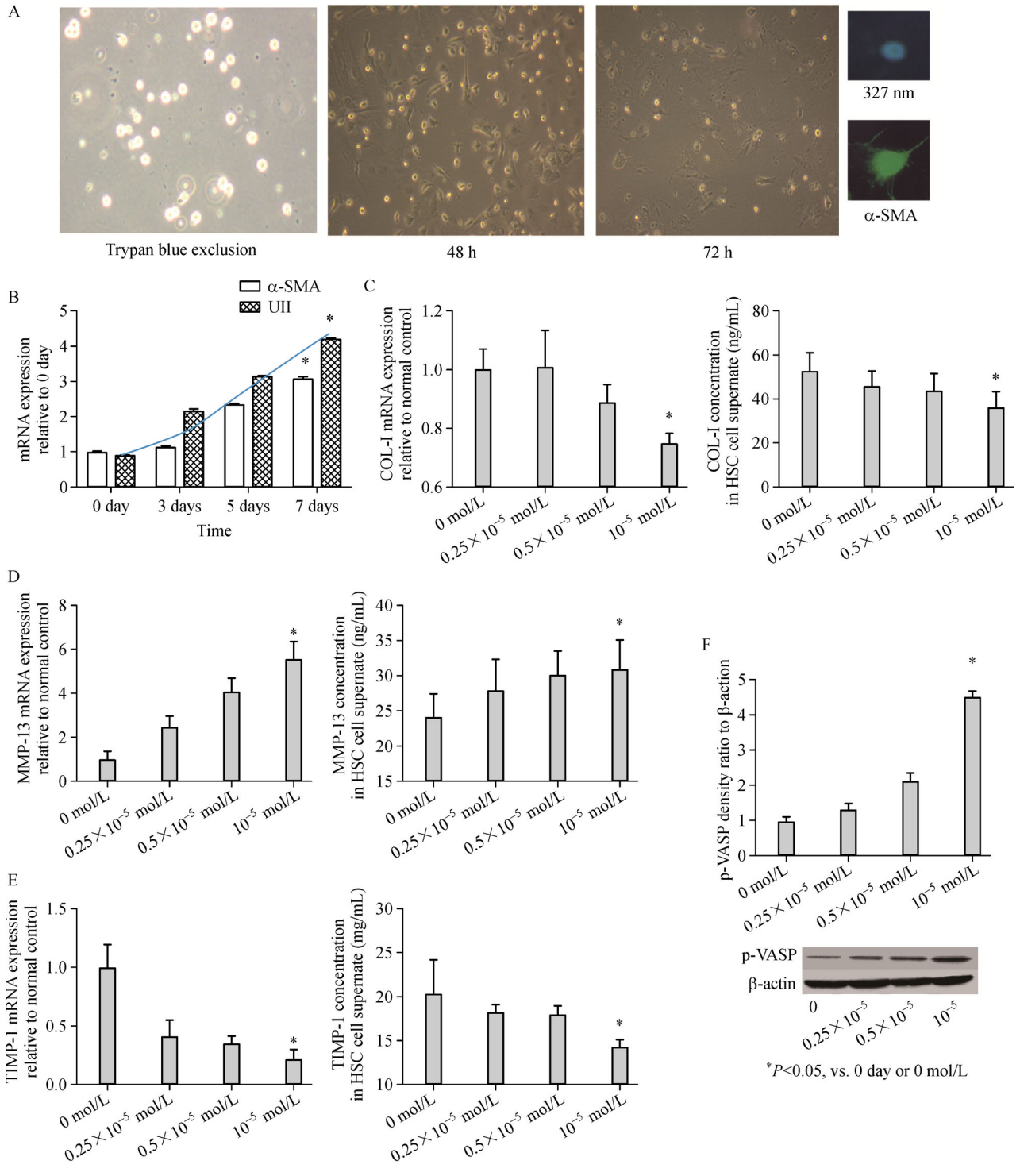

Fig. 3 Direct effect of palosuran on primary hepatic stellate. mRNA expression was determined by real-time PCR in the HSC cells; protein expression of collagen I, MMP-13, and TIMP-1 in HSC cell supernatant was determined by ELISA. (A) Trypan blue staining (left). Primary HSC at 48 h, 72 h (middle); stimulated at 327 nm wavelength, HSCs had blue–green intrinsic auto fluorescence (right). Fluorescence staining with α-SMA. (B) UII gene expression was upregulated during HSC activation (α-SMA as indicated by the measurement of its activation). (C) Palosuran inhibited HSC COL-I gene expression of HSC and protein expression in HSC cell supernatant. (D, E) Palosuran inhibited the expression of MMP-13 and TIMP-1 mRNA as well as the secretion of MMP-13 and TIMP-1mRNA in HSC cells. (F) Protein levels of p-VASP in HSC were quantified by Western blot; palosuran increased the protein levels of p-VASP in a dose-dependent manner. *$P < 0.05$ (10^{-5} mol/L).

attributed to a marked amelioration in fibrosis and a reduced hepatic vascular tone. However, numerous studies, for example, Trebicka *et al.*, supported that palosuran improved PH by reducing PBF [28–30]. These studies suggested that UII is characterized with divergent effects, which include vasodilatation in the splanchnic and vasoconstrictive potencies in conductive vessels. The different functions may result from the UII receptor, UT. The reason for the different results between our study and these studies is not clear. Perhaps the number of each group was small. Therefore, further studies are necessary.

The study concludes that palosuran decreases liver fibrosis scores and serum markers of liver damage. Thus, palosuran in turn exhibits positive results *in vivo*, and antifibrotic and anti-inflammatory effects are determined. Liver fibrogenesis occurs when activated HSCs produce extracellular matrix (ECM) and secrete proinflammatory cytokines. This is a contributing factor to PH because it causes intrahepatic vasculature contractions [6,31]. An evident improvement is made when CCl_4-cirrhotic subjects are treated with palosuran, which is associated with a remarkable decline in α-SMA-positive cells in animals administered with a UII blocker (palosuran). UII/UT mRNA expression in liver and UII serum levels is decreased in palosuran-treated cirrhotic rats. Consequently, the results show that the administration of UII blocking agents leads to a decline in HSC activation by decreasing UT expression and suppressing UII activation in the liver. This finding is consistent with the results of our previous study [13]. This antagonist's anti-inflammatory effects may be related to a decrease in the production and release of proinflammatory cytokine created by Kupffer cells (KCs) [32] because UT protein is mainly translated in KCs in liver cirrhosis [12].

In addition, UII/UT mRNA expression in liver and UII serum levels is upregulated in cirrhotic rats. For the first time, this study unveils that UII gene expression is upregulated during HSC activation, indicating that active HSCs may be a source of circulating UII.

Two components, ECM degradation and HSC apoptosis, primarily take part in the reversible process [33]. Comparing both factors, the role of HSC has a more powerful influence [34]. HSCs also generate a small amount of matrix metalloproteinases and their inhibitors, which are involved in the production and degradation of the ECM [35]. However, an imbalance occurs between the creation of matrix-degrading metalloproteinases and their inhibitors, which in turn cause a matrix accumulation. Our report describes for the first time the effects of palosuran on reducing fibrosis in a pathology with exaggerated collagen deposition. The underlying molecular mechanisms leading to fibrosis regression reveal an increase in the ratio of MMP13-to-TIMP-1 compared with vehicle-treated cirrhotic rats. UII also profoundly impresses the process of fibrosis by the mechanism that leads to the expression of potent cytokines, such as TGF-β1. Palosuran-mediated HSC deactivation may result from the antagonist's capability to activate TGF-β1, a well-known pro-fibrogenic stimulus [36,37].

IHR is also affected by functional components. The molecular mechanism of the palosuran-mediated decrease in intrahepatic vascular resistance is also investigated in the study. Primary HSCs are small and characterized with blue-green intrinsic autofluorescence when they are stimulated at a 327 nm wavelength. To evaluate the effect of palosuran on HSCs *in vitro*, the cells are first cultured with 0 mol/L, 0.25×10^{-5} mol/L, 0.5×10^{-5} mol/L, and 1×10^{-5} mol/L of palosuran for 24 h. UII gene expression is upregulated during HSC activation (α-SMA as indicated by measurement of its activation). After an incubation period of 7 days, the α-SMA positive cells are significantly upregulated compared with 0 day, and associated UII expression increased to 400% compared with freshly isolated cells (Fig. 3B; $P < 0.05$). Therefore, we hypothesize that a relationship may exist between the active HSCs and UII expression. Nitric oxide (NO) plays an essential role in modulating vascular tone within a subject having cirrhosis of the liver [33]. We also characterize the effect of palosuran exhibited on PKG and NO activity, which is a well-known mechanism for HSC relaxation [34]. Our results show that palosuran increases hepatic p-VASP in the cirrhotic model and HSCs, which is a surrogate for PKG activity. Palosuran also increases p-eNOS as an indicator of increased eNOS activity in the cirrhotic model. This suggests that NO has a common pathway that works through p-eNOS and subsequently activates PKG, which induces an increased myosin light-chain phosphatase activity and subsequent HSC relaxation. This may be an additional method by which palosuran decreases hepatic vascular resistance. The recent study by Trebicka *et al.* [38] suggested that increased IHR and hepatic hypertension partly result from increased Rho A/Rho-kinase signaling and decreased NO availability. Moreover, HSCs regulate IHR. They then investigated the effects of statins in cirrhosis rats and HSCs. The results showed statins significantly decrease Rho-kinase activity without affecting expression of RhoA, Rho-kinase, and Ras. In activated HSCs, statins inhibit the membrane association of RhoA and Ras. Furthermore, in cirrhosis rats, statins significantly increase hepatic endothelial nitric oxide synthase (eNOS) mRNA and protein levels, phospho-eNOS, nitrite/nitrate, and the activity of the NO effector PKG.

In summary, this study discovers new evidence that UT antagonists, such as palosuran, may have an important therapeutic role in PH. Overall, palosuran-treated subjects experience improved liver function and decreased hepatic PP through a reduction of intrahepatic vascular resistance without deleterious systemic hemodynamic effects.

Acknowledgements

This study was supported by the National Natural Science Foundation of China (No. 81170408 to Diangang Liu), the Wang Baoen Liver Fibrosis Research Foundation of the China Hepatitis Prevention Foundation (No. 20120124 to Diangang Liu), and the China Postdoctoral Science Foundation (No. 2012M510094 to Diangang Liu).

Compliance with ethics guidelines

Ruoxi Zhang, Jing Chen, Diangang Liu, and Yu Wang declare that they have no conflicts of interest. All institutional and national guidelines for the care and use of laboratory animals were followed.

References

1. Groszmann RJ, Abraldes JG. Portal hypertension: from bedside to bench. J Clin Gastroenterol 2005; 39(4 Suppl 2): S125–S130
2. McConnellM, IwakiriY. Biology of portal hypertension. Hepatol Int 2018; 12(Suppl 1):11–23
3. Vilaseca M, García-Calderó H, Lafoz E, García-Irigoyen O, Avila MA, Reverter JC, Bosch J, Hernández-Gea V, Gracia-Sancho J, García-Pagán JC. The anticoagulant rivaroxaban lowers portal hypertension in cirrhotic rats mainly by deactivating hepatic stellate cells. Hepatology 2017; 65(6): 2031–2044
4. Vilaseca M, García-Calderó H, Lafoz E, Ruart M, López-Sanjurjo CI, Murphy MP, Deulofeu R, Bosch J, Hernández-Gea V, Gracia-Sancho J, García-Pagán JC. Mitochondria-targeted antioxidant mitoquinone deactivates human and rat hepatic stellate cells and reduces portal hypertension in cirrhotic rats. Liver Int 2017; 37(7): 1002–1012
5. Rockey DC, Fouassier L, Chung JJ, Carayon A, Vallee P, Rey C, Housset C. Cellular localization of endothelin-1 and increased production in liver injury in the rat: potential for autocrine and paracrine effects on stellate cells. Hepatology 1998; 27(2): 472–480
6. Iwakiri Y. Pathophysiology of portal hypertension. Clin Liver Dis 2014; 18(2): 281–291
7. Nishimura Y, Ito T, Hoe K, Saavedra JM. Chronic peripheral administration of the angiotensin II AT(1) receptor antagonist candesartan blocks brain AT(1) receptors. Brain Res 2000; 871(1): 29–38
8. Ames RS, Sarau HM, Chambers JK, Willette RN, Aiyar NV, Romanic AM, Louden CS, Foley JJ, Sauermelch CF, Coatney RW, Ao Z, Disa J, Holmes SD, Stadel JM, Martin JD, Liu WS, Glover GI, Wilson S, McNulty DE, Ellis CE, Elshourbagy NA, Shabon U, Trill JJ, Hay DW, Ohlstein EH, Bergsma DJ, Douglas SA. Human urotensin-II is a potent vasoconstrictor and agonist for the orphan receptor GPR14. Nature 1999; 401(6750): 282–286
9. Ross B, McKendy K, Giaid A. Role of urotensin II in health and disease. Am J Physiol Regul Integr Comp Physiol 2010; 298(5): R1156–R1172
10. Thanassoulis G, Huyhn T, Giaid A. Urotensin II and cardiovascular diseases. Peptides 2004; 25(10): 1789–1794
11. Kemp W, Roberts S, Krum H. Increased circulating urotensin II in cirrhosis: potential implications in liver disease. Peptides 2008; 29 (5): 868–872
12. Liu D, Chen J, Wang J, Zhang Z, Ma X, Jia J, Wang Y. Increased expression of urotensin II and GPR14 in patients with cirrhosis and portal hypertension. Int J Mol Med 2010; 25(6): 845–851
13. Liu DG, Wang J, Zhang ZT, Wang Y. The urotension II antagonist SB-710411 arrests fibrosis in CCl_4 cirrhotic rats. Mol Med Rep 2009; 2(6): 953–961
14. Clozel M, Binkert C, Birker-Robaczewska M, Boukhadra C, Ding SS, Fischli W, Hess P, Mathys B, Morrison K, Müller C, Müller C, Nayler O, Qiu C, Rey M, Scherz MW, Velker J, Weller T, Xi JF, Ziltener P. Pharmacology of the urotensin-II receptor antagonist palosuran (ACT-058362; 1-[2-(4-benzyl-4-hydroxy-piperidin-1-yl)-ethyl]-3-(2-methyl-quinolin-4-yl)-urea sulfate salt): first demonstration of a pathophysiological role of the urotensin system. J Pharmacol Exp Ther 2004; 311(1): 204–212
15. Mejias M, Coch L, Berzigotti A, Garcia-Pras E, Gallego J, Bosch J, Fernandez M. Antiangiogenic and antifibrogenic activity of pigment epithelium-derived factor (PEDF) in bile duct-ligated portal hypertensive rats. Gut. 2015; 64(4): 657–666
16. Clozel M, Hess P, Qiu C, Ding SS, Rey M. The urotensin-II receptor antagonist palosuran improves pancreatic and renal function in diabetic rats. J Pharmacol Exp Ther 2006; 316(3): 1115–1121
17. Hsu SJ, Lee FY, Wang SS, Hsin IF, Lin TY, Huang HC, Chang CC, Chuang CL, Ho HL, Lin HC, Lee SD. Caffeine ameliorates hemodynamic derangements and portosystemic collaterals in cirrhotic rats. Hepatology 2015; 61(5): 1672–1684
18. Delgado MG, Gracia-Sancho J, Marrone G, Rodríguez-Vilarrupla A, Deulofeu R, Abraldes JG, Bosch J, García-Pagán JC. Leptin receptor blockade reduces intrahepatic vascular resistance and portal pressure in an experimental model of rat liver cirrhosis. Am J Physiol Gastrointest Liver Physiol 2013; 305(7): G496–G502
19. Darlington AS, Dippel DW, Ribbers GM, van Balen R, Passchier J, Busschbach JJ. A prospective study on coping strategies and quality of life in patients after stroke, assessing prognostic relationships and estimates of cost-effectiveness. J Rehabil Med 2009; 41(4): 237–241
20. Mülsch A, Oelze M, Klöss S, Mollnau H, Töpfer A, Smolenski A, Walter U, Stasch JP, Warnholtz A, Hink U, Meinertz T, Münzel T. Effects of *in vivo* nitroglycerin treatment on activity and expression of the guanylyl cyclase and cGMP-dependent protein kinase and their downstream target vasodilator-stimulated phosphoprotein in aorta. Circulation 2001; 103(17): 2188–2194
21. Schmittgen TD, Livak KJ. Analyzing real-time PCR data by the comparative C(T) method. Nat Protoc 2008; 3(6): 1101–1108
22. Ramm GA. Isolation and culture of rat hepatic stellate cells. J Gastroenterol Hepatol 1998; 13(8): 846–851
23. Rockey DC, Weisiger RA. Endothelin induced contractility of stellate cells from normal and cirrhotic rat liver: implications for regulation of portal pressure and resistance. Hepatology 1996; 24 (1): 233–240
24. Liu J, Gong H, Zhang ZT, Wang Y. Effect of angiotensin II and angiotensin II type 1 receptor antagonist on the proliferation, contraction and collagen synthesis in rat hepatic stellate cells. Chin Med J (Engl) 2008; 121(2): 161–165
25. Kemp W, Krum H, Colman J, Bailey M, Yandle T, Richards M, Roberts S. Urotensin II: a novel vasoactive mediator linked to chronic liver disease and portal hypertension. Liver Int 2007; 27(9):

1232–1239
26. Kemp W, Kompa A, Phrommintikul A, Herath C, Zhiyuan J, Angus P, McLean C, Roberts S, Krum H. Urotensin II modulates hepatic fibrosis and portal hemodynamic alterations in rats. Am J Physiol Gastrointest Liver Physiol 2009; 297(4): G762–G767
27. Sidharta PN, Rave K, Heinemann L, Chiossi E, Krähenbühl S, Dingemanse J. Effect of the urotensin-II receptor antagonist palosuran on secretion of and sensitivity to insulin in patients with type 2 diabetes mellitus. Br J Clin Pharmacol 2009; 68(4): 502–510
28. Trebicka J, Leifeld L, Hennenberg M, Biecker E, Eckhardt A, Fischer N, Pröbsting AS, Clemens C, Lammert F, Sauerbruch T, Heller J. Hemodynamic effects of urotensin II and its specific receptor antagonist palosuran in cirrhotic rats. Hepatology 2008; 47 (4): 1264–1276
29. Heller J, Schepke M, Neef M, Woitas R, Rabe C, Sauerbruch T. Increased urotensin II plasma levels in patients with cirrhosis and portal hypertension. J Hepatol 2002; 37(6): 767–772
30. Leifeld L, Clemens C, Heller J, Trebicka J, Sauerbruch T, Spengler U. Expression of urotensin II and its receptor in human liver cirrhosis and fulminant hepatic failure. Dig Dis Sci 2010; 55(5): 1458–1464
31. YadavL, PuriN, RastogiV, SatputeP, AhmadR, KaurG. Matrix metalloproteinases and cancer-roles in threat and therapy. Asian Pac J Cancer Prev 2014; 15(3): 1085–1091
32. Liu LM, Liang DY, Ye CG, Tu WJ, Zhu T. The UII/UT system mediates upregulation of proinflammatory cytokines through p38 MAPK and NF-κB pathways in LPS-stimulated Kupffer cells. PLoS One 2015; 10(3): e0121383
33. Wiest R, Groszmann RJ. The paradox of nitric oxide in cirrhosis and portal hypertension: too much, not enough. Hepatology 2002; 35(2): 478–491
34. Verbeke L, Farre R, Trebicka J, Komuta M, Roskams T, Klein S, Elst IV, Windmolders P, Vanuytsel T, Nevens F, Laleman W. Obeticholic acid, a farnesoid X receptor agonist, improves portal hypertension by two distinct pathways in cirrhotic rats. Hepatology 2014; 59(6): 2286–2298
35. MallatA, LotersztajnS. Targeting cannabinoid receptors in hepatocellular carcinoma. Gut 2016; 65(10):1582–1583
36. Cheng K, Yang N, Mahato RI. TGF-β1 gene silencing for treating liver fibrosis. Mol Pharm 2009; 6(3): 772–779
37. Chen RJ, Wu HH, Wang YJ. Strategies to prevent and reverse liver fibrosis in humans and laboratory animals. Arch Toxicol 2015; 89 (10): 1727–1750
38. Trebicka J, Hennenberg M, Laleman W, Shelest N, Biecker E, Schepke M, Nevens F, Sauerbruch T, Heller J. Atorvastatin lowers portal pressure in cirrhotic rats by inhibition of RhoA/Rho-kinase and activation of endothelial nitric oxide synthase. Hepatology 2007; 46(1): 242–253